Appearance of Antiferromagnetic Dipole Order in $Ce_{0.5}La_{0.5}B_6$ with Pr Ion Doping

Takeshi Matsumura[1,2], Keisuke Kunimori[1], Akihiro Kondo[3], Kei Soejima[1], Hiroshi Tanida[1], Jean-Michel Mignot[4], Fumitoshi Iga[5], and Masafumi Sera[1,2]

[1]*Department of Quantum Matter, AdSM, Hiroshima University, Higashi-Hiroshima, Hiroshima 739-8530*
[2]*Institute for Advanced Materials Research, Hiroshima University, Higashi-Hiroshima, Hiroshima 739-8530*
[3]*Institute for Solid State Physics, University of Tokyo, Kashiwa, Chiba 277-8581*
[4]*Laboratoire Léon Brillouin, CEA-CNRS, CEA/Saclay, 91191 Gif sur Yvette, France*
[5]*Faculty of Science, Ibaraki University, Mito, Ibaraki 310-8512*

We have performed a neutron diffraction experiment on Pr-doped $Ce_{0.5}Pr_{0.1}La_{0.4}B_6$, in which an antiferromagnetic octupole order with $\boldsymbol{q} = (\frac{1}{2}, \frac{1}{2}, \frac{1}{2})$ could be anticipated by analogy with $Ce_{0.7}La_{0.3}B_6$. Contrary to this natural expectation, we detected an unambiguous magnetic peak at $\boldsymbol{q} = (\frac{1}{4}, \frac{1}{4}, \frac{1}{2})$, which is the same $\boldsymbol{q}$-vector frequently realized in the magnetic ordered phases of RB_6 (R=rare earth) compounds. No significant signal was observed at $\boldsymbol{q} = (\frac{1}{2}, \frac{1}{2}, \frac{1}{2})$ at zero magnetic field. This result shows that the normal antiferromagnetic dipole moment is also one of the competing multipole order parameters in the $Ce_xLa_{1-x}B_6$ system. The relevant order parameters are close in energy and can be tuned by a weak perturbation.

Journal Ref: J. Phys. Soc. Jpn., **83**, 094724 (2014).
http://dx.doi.org/10.7566/JPSJ.83.094724

1. Introduction

Interionic exchange interactions involving multipole degrees of freedom give rise to a wide variety of unconventional ordered phases in f-electron systems. One of the typical examples is the lanthanum-doped cerium hexaboride $Ce_xLa_{1-x}B_6$.[1–6] The crystal-field ground state of the Ce ion is the Γ_8 quartet, having three magnetic dipole moments, five electric quadrupole moments, and seven magnetic octupole moments. All of them are active and their interactions have comparable magnitudes.[7,8] For $x > 0.75$, the ordered phase at the lowest temperature is described by the superposition of an antiferromagnetic dipole (AFM) order developing on an underlying antiferroelectric quadrupole (AFQ) order. The paramagnetic phase, AFQ phase, and AFM phase, appearing with decreasing temperature, have been named phases I, II, and III, respectively. The order parameter of the AFQ phase is a combination of O_{yz}-, O_{zx}-, and O_{xy}-type (Γ_{5g}) quadrupole moments with a propagation vector $\boldsymbol{q}_0 = (\frac{1}{2}, \frac{1}{2}, \frac{1}{2})$, which has been directly detected by X-ray diffraction in CeB_6.[9–13] In magnetic fields, T_{xyz}-type (Γ_{2u}) antiferromagnetic octupole (AFO) moments are induced with the same $\boldsymbol{q}_0$ vector. The magnetic structure of the AFM order in the O_{xy}-AFQ domain is described by a non-collinear double-$\boldsymbol{q}$-$\boldsymbol{q}'$ structure with $\boldsymbol{q}_1 = (\frac{1}{4}, \frac{1}{4}, \frac{1}{2})$, $\boldsymbol{q}_2 = (\frac{1}{4}, \frac{\bar{1}}{4}, \frac{1}{2})$, $\boldsymbol{q}'_1 = (\frac{1}{4}, \frac{1}{4}, 0)$, and $\boldsymbol{q}'_2 = (\frac{1}{4}, \frac{\bar{1}}{4}, 0)$, which shows that the magnetic structure is strongly affected by the underlying AFQ order, although its detailed structure is still under study.[14–18]

Interest in $Ce_xLa_{1-x}B_6$ has been stimulated by the appearance of another type of ordered phase for $x \leq 0.8$, which has been named "phase IV" and is considered to be an AFO phase with the $(T_x^\beta + T_y^\beta + T_z^\beta)$-type ($\Gamma_{5u}$) order parameter. Although this is convincingly established by resonant X-ray diffraction experiments,[19–23] there still remain a few problems concerning the behavior in magnetic fields.[24] One is that the cusp anomaly in the magnetic susceptibility cannot be explained by a mean-field calculation assuming the Γ_{5u}-AFO order if one includes the Γ_{5g}-AFQ interaction that should exist intrinsically in the $Ce_xLa_{1-x}B_6$ system. Regarding this issue, it has recently been pointed out that the Γ_{5g}-AFQ order is induced by the field in the Γ_{5u}-AFO phase much more strongly than expected from the mean-field model, which predicts, contrastingly, that the Γ_{3g}-AFQ (O_{20} and O_{22}) order should be induced most strongly.[23] This is the reason for the above discrepancy and we consider that fluctuations of the Γ_{5g}-AFQ order parameters exist behind the Γ_{5u}-AFO order, which are not included in the mean-field model.

Another problem concerning phase IV is that the AFO transition temperature increases when Pr or Nd is doped into $Ce_xLa_{1-x}B_6$ for x=0.4 and 0.5.[25] For $x = 0.5$, the transition temperature increases from 0.8 K in $Ce_{0.5}La_{0.5}B_6$ to 1.7 K in $Ce_{0.5}Pr_{0.1}La_{0.4}B_6$. The increase is larger for Pr doping than for Nd doping, despite the fact that the Γ_5-triplet crystal-field ground state of Pr^{3+} does not possess an octupolar degree of freedom. From this result, the authors discussed that the AFO phase may be coupled with the magnetic dipolar degree of freedom and thereby become stabilized, which is contradictory to the current scenario of a pure Γ_{5u}-AFO order.[25]

We consider that these problems in the Γ_{5u}-AFO phase of $Ce_xLa_{1-x}B_6$ are associated with the competing nature of various types of possible multipolar order parameters, the understanding of which is one of the principal goals of our study. Concerning the effect of magnetic ion doping, however, since there is no microscopic evidence of the AFO order in doped compounds, it is necessary to check whether the ordered phase in doped compounds is actually the same AFO phase as that

in $Ce_{0.7}La_{0.3}B_6$, as previously supposed. For this purpose, we performed a neutron diffraction experiment on Pr-doped $Ce_{0.5}Pr_{0.1}La_{0.4}B_6$, which has a relatively high transition temperature. We contrastingly found that the ordered phase of $Ce_{0.5}Pr_{0.1}La_{0.5}B_6$ is not the AFO phase, but clearly the AFM phase. After describing the experimental procedure in Sect. 2, the results of neutron diffraction are presented in Sect. 3. Then, we propose a temperature vs concentration phase diagram of the magnetic ion doping system $Ce_xR_yLa_{1-x-y}B_6$ for R=Nd and Pr, and discuss the competing nature of the order parameters.

2. Experimental Procedure

Single crystals of $Ce_{0.5}Pr_{0.1}La_{0.4}B_6$ were grown by the floating-zone method using an image furnace with four xenon lamps.[26] An enriched ^{11}B isotope was used to reduce the absorption of neutrons by ^{10}B contained in natural boron.

One neutron diffraction experiment was performed using the triple-axis thermal neutron spectrometer TOPAN installed at the beam port 6G of the research reactor JRR-3, Japan Atomic Energy Agency, Tokai, Japan. Incident neutrons with $\lambda = 1.41$ Å were selected using the 002 Bragg reflection of pyrolytic graphite (PG) crystals. The wavelength of the scattered beam was also analyzed (1.41 Å) using a PG-002 crystal analyzer. Neutrons with higher harmonic energies were eliminated by PG filters placed before and after the sample. The condition of the horizontal collimators was open-60′-60′-open. The experiment was performed at zero magnetic field, using a Joule-Thomson-type ^3He gas closed-cycle refrigerator.

To gain intensity, two cylindrical sample pieces, with masses of 1.070 and 0.485 g, were aligned together. The $[1\bar{1}0]$ axis of the crystal was almost parallel to the cylinder axis, and the samples were oriented so that the [110] and [001] axes spanned the scattering plane. The misalignment between the two pieces of samples was less than 0.5° and the final width of the rocking scan for the nuclear Bragg peaks was $\sim 0.6°$.

A neutron diffraction experiment was also performed using the 6T2 diffractometer at the reactor Orphée of Laboratoire Léon Brillouin, Saclay, France. We used a lifting counter system to study the reciprocal space outside the horizontal scattering plane. The same 1.070 g sample was attached to a dilution refrigerator in a cryomagnet. A magnetic field was applied along the $[1\bar{1}0]$ axis. Incident neutrons with $\lambda = 0.91$ Å were selected using a copper monochromator. A 20′ collimator was inserted before the counter to reduce the background.

3. Results and Discussion

3.1 AFM dipole order

We first show that the reflections corresponding to the AFO order with $\boldsymbol{q}_0 = (\frac{1}{2}, \frac{1}{2}, \frac{1}{2})$ observed in $Ce_{0.7}La_{0.3}B_6$ were not detected within the experimental accuracy of the present experiment. Figure 1 shows an example of the rocking scans performed under nearly the same conditions as those in Ref. 22. Even if we take into account the possibly weaker intensity due to the lower Ce concentration than in $Ce_{0.7}La_{0.3}B_6$, we expect at least 250

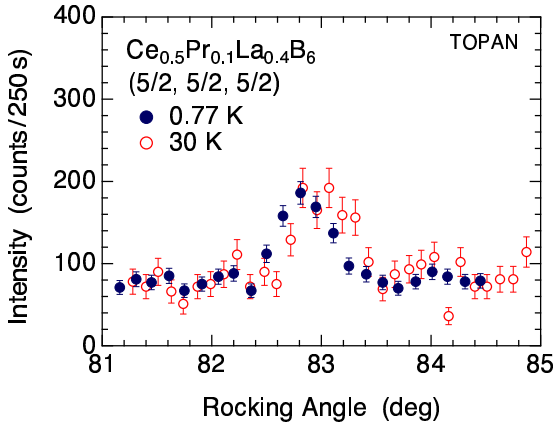

Fig. 1. (Color online) Rocking scans at $(\frac{5}{2}, \frac{5}{2}, \frac{5}{2})$. The peak is due to the residual $\lambda/2$ contamination in the incident beam.

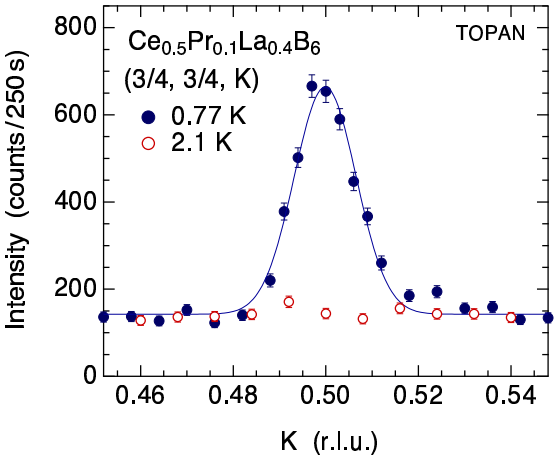

Fig. 2. (Color online) Peak profiles of the $(\frac{3}{4}, \frac{3}{4}, \frac{1}{2})$ magnetic Bragg reflection below and above the transition temperature.

counts per 250 s in this scan, which is sufficiently large to be detected above the background. Therefore, we can conclude from this negative result, and also from the clear magnetic dipole signals shown next, that *the AFO order is not realized* in $Ce_{0.5}Pr_{0.1}La_{0.4}B_6$.

Figure 2 shows the peak profile of the magnetic Bragg reflection at the scattering vector $\boldsymbol{Q} = (\frac{3}{4}, \frac{3}{4}, \frac{1}{2})$, which disappears above the transition temperature. This corresponds to the propagation vector $\boldsymbol{q}_1 = (\frac{1}{4}, \frac{1}{4}, \frac{1}{2})$, which is widely observed in the antiferromagnetic ordered phases in the RB_6 series except NdB_6.[27–31] Figure 3 shows the temperature dependence of the peak-top intensity of the $(\frac{3}{4}, \frac{3}{4}, \frac{1}{2})$ reflection. The intensity shows a clear anomaly at the transition temperature of 1.7 K, which is consistent with the result of specific heat measurement reported in Ref. 25.

Here, we emphasize the unusual temperature dependence of the intensity, increasing gradually below 1.7 K and more steeply at lower temperatures. We consider that this behavior is associated with the characteristic shape of the specific heat anomaly reported in Ref. 25; $C(T)$ shows a convex temperature dependence below 1.7

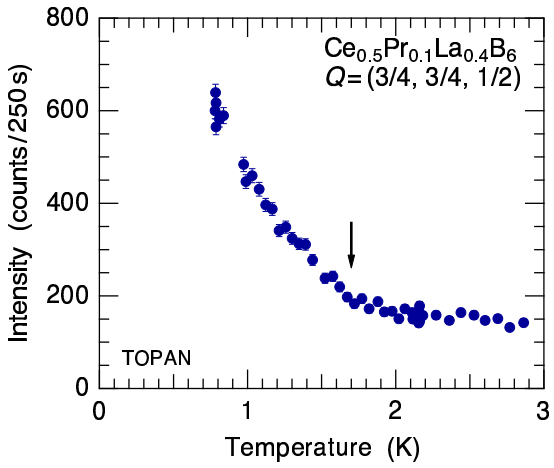

Fig. 3. (Color online) Temperature dependence of the peak-top intensity of the $(\frac{3}{4}, \frac{3}{4}, \frac{1}{2})$ magnetic Bragg reflection. The arrow indicates the transition temperature.

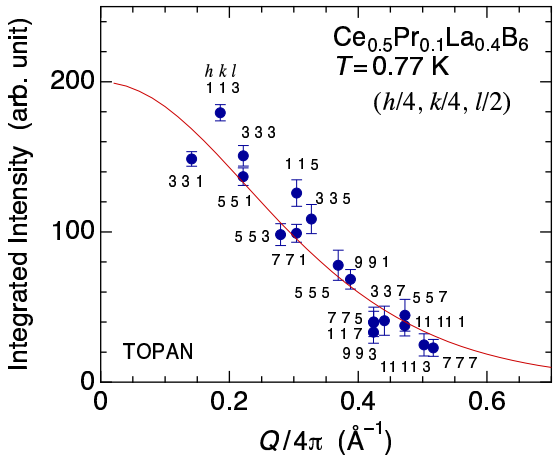

Fig. 4. (Color online) Q dependence of the Lorentz-factor-corrected intensities of the $\langle \frac{1}{4}, \frac{1}{4}, \frac{1}{2} \rangle$-equivalent reflections. The solid line shows $|f(Q)|^2$ in the dipole approximation averaged for the Ce and Pr compositions.

K. We suggest that the development of the long-range order is hampered by Pr doping, especially in the region near the transition temperature. This may be a consequence of a complex interplay between different magnetic interactions originating from Pr and Ce, causing the order parameter to develop in an unusual manner as in $Ce_xPr_{1-x}B_6$.[32]

Figure 4 shows the scattering vector ($\boldsymbol{Q}$) dependence of the intensity for 18 equivalent Bragg reflections in the [110]-[001] scattering plane. The integrated intensities for the rocking scans were corrected for the Lorentz factor $\sin 2\theta$. As shown in Fig. 4, the intensity decreases with increasing Q and follows a curve representing a normal magnetic form factor of the Ce^{3+} and Pr^{3+} ions. Here, the magnetic form factor $f(Q)$ in the dipole approximation is expressed as

$$f(Q) = \langle j_0 \rangle + (\frac{2}{g} - 1)\langle j_2 \rangle. \quad (1)$$

We used the calculated radial integrals of $\langle j_0 \rangle$ and $\langle j_2 \rangle$.[33] The solid line in Fig. 4 shows $|f(Q)|^2$, where $f(Q)$ is averaged with respect to the Ce and Pr compositions. We note that the difference between f_{Ce} and f_{Pr} is much smaller than the scatter of the data points in Fig. 4.

If the magnetic structure were the same as that of CeB_6, the Bragg peaks of $\langle \frac{1}{4}, \frac{1}{4}, 0 \rangle$ should be observed because of the underlying AFQ order. However, within the present experimental accuracy, we could not detect magnetic peaks at $\langle \frac{1}{4}, \frac{1}{4}, 0 \rangle$-equivalent positions. This result shows that the AFQ order does not exist at zero field.

To obtain information on a possible magnetic structure and on the value of the ordered moment, we calculated the magnetic structure factors for two possible structural models. The magnetic moment $\boldsymbol{\mu}_i$ of the magnetic ion at $\boldsymbol{r}_i$ is written as

$$\boldsymbol{\mu}_i = \sum_j \boldsymbol{m}_j \cos(\boldsymbol{q}_j \cdot \boldsymbol{r}_i + \varphi_j), \quad (2)$$

where $\boldsymbol{q}_j$ is the jth member of the multi-$\boldsymbol{q}$ components, and $\boldsymbol{m}_j$ and φ_j are the Fourier component and phase factor for $\boldsymbol{q}_j$, respectively. In the present case, the magnetic unit cell consists of $4 \times 4 \times 2$ crystallographic unit cells, and 32 rare-earth sites are taken into account. The magnetic structure factor $F_M(\boldsymbol{Q})$ is written as

$$F_M(\boldsymbol{Q}) = \sum_i \frac{1}{2} f(Q)\{\tilde{\boldsymbol{Q}} \times (\boldsymbol{\mu_i} \times \tilde{\boldsymbol{Q}})\} e^{-i\boldsymbol{Q}\cdot\boldsymbol{r}_i}, \quad (3)$$

where $\tilde{\boldsymbol{Q}}$ represents the unit vector of $\boldsymbol{Q}$.

If we assume a single-$\boldsymbol{q}$ structure with $\boldsymbol{q}_1 = (\frac{1}{4}, \frac{1}{4}, \frac{1}{2})$, $\boldsymbol{m}_1$ should be along $[1\bar{1}0]$ to explain the data points in Fig. 4. In this case, the moments are perpendicular to the scattering plane, and the calculated intensity lies exactly on the solid line in Fig. 4, providing the closest agreement with the experimental data points. We consider that the scatter around the solid line is the systematic error due to the difference in the geometrical conditions of the sample. The error bars in Fig. 4 represent only the statistical error of one sigma. If we change the direction of the moment, although the calculated intensities scatter around the solid line, the consistency with the data is not improved. Finally, in order for all the moments to have the same magnitude, the phase factor φ_1 should be $\pi/4$.

By assuming a double-$\boldsymbol{q}$ structure with $\boldsymbol{q}_1 = (\frac{1}{4}, \frac{1}{4}, \frac{1}{2})$ and $\boldsymbol{q}_2 = (\frac{1}{4}, \bar{\frac{1}{4}}, \frac{1}{2})$, the same intensity curve is obtained by setting $\boldsymbol{m}_1 \parallel [1\bar{1}0]$ and $\boldsymbol{m}_2 \parallel [110]$. In addition, if we set $\phi_1 = 0$ and $\phi_2 = \pi/2$, the magnetic structure becomes identical to that of PrB_6. As proposed for the incommensurate ordered phase in $Ce_xPr_{1-x}B_6$, this double-$\boldsymbol{q}$ structure is considered to be associated with the AFQ interaction induced by the Pr doping.[32] In any case, we cannot distinguish between the single-$\boldsymbol{q}$ and double-$\boldsymbol{q}$ structures from the zero-field data alone. We will come back to this point in the discussion of magnetic field effects in Sect. 3.2.

The magnitude of the ordered moment has been estimated by comparing the intensities with those of nuclear reflections. All the fifteen hhl reflections with $2\theta < 100°$

were used for reference, whose intensities were roughly proportional to the calculated intensities. If we assume the single-$\boldsymbol{q}$ structure mentioned above, there appear six domains with equivalent $\boldsymbol{q}$-vectors, i.e., $\boldsymbol{q} = (\pm\frac{1}{4}, \frac{1}{4}, \frac{1}{2})$, $(\pm\frac{1}{4}, \frac{1}{2}, \frac{1}{4})$, and $(\frac{1}{2}, \pm\frac{1}{4}, \frac{1}{4})$. We observe only one of them in the present scattering plane. Furthermore, the substitution of La reduces the intensity by a factor $(0.5+0.1)^2$. If we assume that Ce and Pr ions have an average magnitude of the magnetic moment, $\mu = 0.3 \pm 0.1\ \mu_B$ per Ce or Pr ion. The same value is obtained by assuming the double-$\boldsymbol{q}$ structure.

In reality, the moments of Ce and Pr ions, μ_{Ce} and μ_{Pr}, should be different because 2 μ_B is expected for the Γ_5 ground state of Pr^{3+} and 1.57 μ_B for the Γ_8 ground state of Ce^{3+}. Furthermore, μ_{Ce} is expected to be reduced owing to the Kondo effect. In the AFM phase of pure CeB_6, μ_{Ce} is estimated to be $0.28 \pm 0.06\ \mu_B$.[14] As to μ_{Pr}, we refer to the averaged moment value for the $Ce_xPr_{1-x}B_6$ system, which increases from 0.8 μ_B at $x = 0.8$ to 1.9 μ_B at $x = 0.2$, which are considered to be mostly due to Pr.[32] Therefore, the moment of Pr is expected to be larger than that of Ce. In the present case, if we ascribe all the moments to Pr ions only, assuming that Ce ions are paramagnetic, μ_{Pr} is estimated to be 1.8 μ_B, which is consistent with the value expected for the Γ_5 ground state. However, such a situation is hardly expected because a concentration of only 10% is too low to realize the AFM order.[34] Both Ce and Pr ions should contribute to the ordering. Therefore, the estimated average $\mu = 0.3 \pm 0.1\ \mu_B$ should be interpreted as the maximum moment allowed for Ce^{3+}. If we attribute 1.0 μ_B for Pr^{3+}, μ_{Ce} is estimated to be $0.17 \pm 0.1\ \mu_B$.

3.2 Magnetic field dependence

In this subsection, we show experimental results supporting the single-$\boldsymbol{q}$ AFM order at zero field. The main results concerning the magnetic structure are presented in Sect. 3.2.1 and 3.2.2. In Sects. 3.2.3 and 3.2.4, we address more complex aspects of magnetic domain repopulation, irreversibilities, and the possible coexistence of AFM and AFQ orders. Although the precise AFM structure at zero field has not been determined in Sect. 3.1, it is very likely that the Fourier component $\boldsymbol{m}_j$ is perpendicular to $\boldsymbol{q}_j$. We use this information to interpret the magnetic field effects.

3.2.1 Experimental results

To distinguish between the single-$\boldsymbol{q}$ and multi-$\boldsymbol{q}$ magnetic structures, and also to investigate the domain motion in magnetic fields, we measured the field dependences of the intensities of selected magnetic peaks. The results are shown in Fig. 5. In the initial zero-field state, all the magnetic peaks corresponding to the magnetic wave vectors $\boldsymbol{q}_{1,2} = (\frac{1}{4}, \pm\frac{1}{4}, \frac{1}{2})$, $\boldsymbol{q}_{3,4} = (\frac{1}{2}, \pm\frac{1}{4}, \frac{1}{4})$, and $\boldsymbol{q}_{5,6} = (\pm\frac{1}{4}, \frac{1}{2}, \frac{1}{4})$ exist. In the first field scan (points labelled "1" in Fig. 5), we measured the $(\frac{5}{4}, \frac{1}{4}, \frac{1}{2})$ and $(\frac{1}{4}, -\frac{1}{4}, \frac{3}{2})$ peaks corresponding to $\boldsymbol{q}_1$ ($\boldsymbol{m}_1 \parallel \boldsymbol{H}$) and $\boldsymbol{q}_2$ ($\boldsymbol{m}_2 \perp \boldsymbol{H}$), respectively. As shown in Fig. 5, the intensity associated with $\boldsymbol{q}_1$ disappeared at 1.8 T, whereas that associated with $\boldsymbol{q}_2$ decreased less steeply, reached a plateau at approximately 2.5 T, then finally dropped to zero at 4 T.

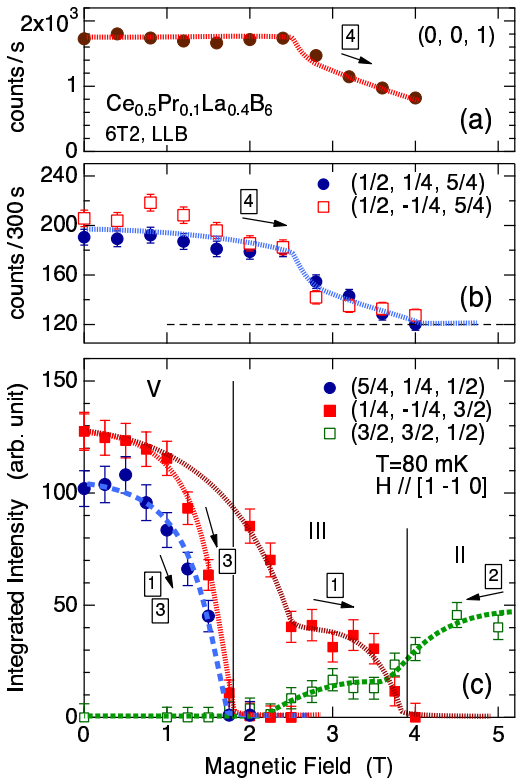

Fig. 5. (Color online) Magnetic field dependences of the intensities of the (a) $(0, 0, 1)$ nuclear peak, (b) $(\frac{1}{2}, \frac{1}{4}, \frac{5}{4})$ and $(\frac{1}{2}, -\frac{1}{4}, \frac{5}{4})$ magnetic peaks, and (c) $(\frac{5}{4}, \frac{1}{4}, \frac{1}{2})$, $(\frac{1}{4}, -\frac{1}{4}, \frac{3}{2})$, and $(\frac{3}{2}, \frac{3}{2}, \frac{1}{2})$ magnetic peaks. The numbers in the square boxes represent the sequence of the scans. The solid and dashed lines are visual guides.

From the magnetic phase diagrams reported in the literature,[25,35–38] the three field regions of $H < 1.8$ T, $1.8 < H < 4$ T, and $H > 4$ T in $Ce_{0.5}Pr_{0.1}La_{0.4}B_6$ for $\boldsymbol{H} \parallel [1\bar{1}0]$ are consistently interpreted as the low-field AFM phase (named "phase V" in Fig. 5), phase III (AFM+AFQ), and phase II (AFQ), respectively.

After returning the field to zero through the scan "2", the same $\boldsymbol{q}_{1,2}$ peaks were measured again in a second field increase (points labelled "3" in Fig. 5). Their intensities started from the same values as those in the first scan, and the $\boldsymbol{q}_1$ peak followed the same curve. But now, the $\boldsymbol{q}_2$ peak also disappeared at the 1.8 T boundary, rather than at 4 T as observed in the first scan. Finally (points labelled "4" in Fig. 5), the $\boldsymbol{q}_{3,4}$ magnetic peaks were measured, together with the (0,0,1) nuclear peak. These magnetic peaks did not exhibit any anomaly at the 1.8 T boundary, but their intensities decreased abruptly at 2.5 T, and vanished at 4 T.

3.2.2 Magnetic structure at zero field

The disappearance of the $\boldsymbol{q}_1$ peak at 1.8 T in the first and third scans is probably because $\boldsymbol{m}_1 \parallel [1\bar{1}0]$ is parallel to the magnetic field. By contrast, the $\boldsymbol{q}_2$ peak persists up to 4 T in the first scan, which may be associated with the preferable condition of $\boldsymbol{m}_2 \perp \boldsymbol{H}$. This result shows that $\boldsymbol{q}_1$ and $\boldsymbol{q}_2$ are decoupled in the first scan. Therefore,

it is likely that the zero-field AFM order can be described by a single-$\boldsymbol{q}$ structure.

In addition, as will be described in Sect. 3.2.4, the AFM component with $\boldsymbol{q}_0 = (\frac{1}{2}, \frac{1}{2}, \frac{1}{2})$, which is induced in phases III and II in association with the AFQ order, vanishes in the low-field phase below 1.8 T, as shown in Fig. 5. Therefore, the AFM order of $Ce_{0.5}La_{0.4}Pr_{0.1}B_6$ in phase V is different from that in phase III in magnetic fields. To emphasize that there is a phase boundary at 1.8 T, we name the low-field phase as "phase V". This is consistent with the magnetic phase diagram reported in Ref. 25.

3.2.3 Domain motion

The anomalies at 2.5 T in phase III are probably associated with the selection of magnetic domains. The decrease in the intensity of the (0,0,1) nuclear peak can be ascribed to the enhancement of the extinction. Since the magnetic domain is coupled with the lattice through the AFQ order, some *disorder* in the lattice, existing at low fields with a multidomain state, can also be suppressed by the selection of magnetic domains, which results in the enhancement of the extinction.

Since the order parameter of phase II for $H \parallel [1\bar{1}0]$ is $\langle O_{yz} - O_{zx} \rangle$ with a single-domain state,[13] the magnetic domain in phase III should be compatible with the O_{yz} and O_{zx} AFQ order; therefore, the $\boldsymbol{q}_{3,4} = (\frac{1}{2}, \pm\frac{1}{4}, \frac{1}{4})$ and $\boldsymbol{q}_{5,6} = (\pm\frac{1}{4}, \frac{1}{2}, \frac{1}{4})$ domains, respectively, are expected to be selected. This is consistent with the fact that the $\boldsymbol{q}_{3,4}$ peaks survive in phase III, as shown in the fourth scan. Note that the $\boldsymbol{q}_{1,2}$ peaks should have disappeared in phase III in the fourth scan, which can be explained by the third scan. In addition, since the Fourier components for $\boldsymbol{q}_3$ ($\boldsymbol{m}_3 \parallel [01\bar{1}]$) and $\boldsymbol{q}_4$ ($\boldsymbol{m}_4 \parallel [011]$) have equivalent relations to the field direction ($H \parallel [1\bar{1}0]$), the $\boldsymbol{q}_3$ and $\boldsymbol{q}_4$ peaks exhibit the same field dependence. The same should be the case for the $\boldsymbol{q}_{5,6}$ peaks. The decrease in the intensity of the $\boldsymbol{q}_{3,4}$ peak at 2.5 T suggests the selection of the $\boldsymbol{q}_{5,6}$ (O_{zx}) domain due to a small misalignment. It is expected that the intensity of the $\boldsymbol{q}_{5,6}$ peak would increase above 2.5 T. However, since we do not have the data for $\boldsymbol{q}_{5,6}$ and since not all peaks have been measured simultaneously, it is unfortunately difficult to describe the domain motion accurately.

The disappearance of the $\boldsymbol{q}_2$ peak at 1.8 T in the third scan could also be associated with the domain selection. When the field is increased up to 5 T in the first scan, the lattice domain preferable for the O_{xy} AFQ order should be wiped out, which existed initially in the first scan up to 4 T with the $\boldsymbol{q}_2$ magnetic domain. If this lattice domain is not recovered after returning to zero field, the $\boldsymbol{q}_2$ magnetic domain could soon be wiped out in the next field increase. Actually, at zero field after the second scan, the intensity of the (0,0,1) nuclear peak was found to have been reduced to approximately 60% of the initial intensity because of the increased extinction. In a similar way, we could also consider a possibility that the double-$\boldsymbol{q}$ structure in phase III is trapped and persists down to $H = 0$. In this case, the $\boldsymbol{q}_1$ and $\boldsymbol{q}_2$ peaks are linked together in the next field increase. However, these interpretations are partly speculative and cannot be ascertained without additional measurements.

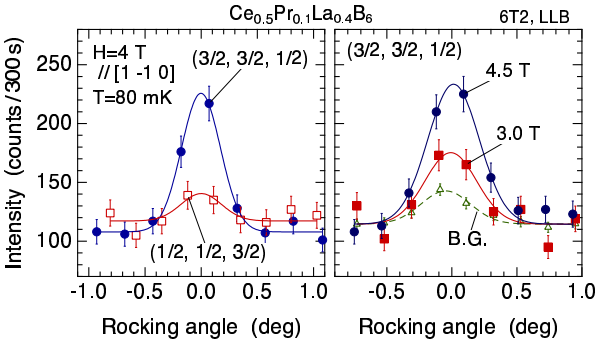

Fig. 6. (Color online) Rocking scans of the $(\frac{3}{2}, \frac{3}{2}, \frac{1}{2})$ and $(\frac{1}{2}, \frac{1}{2}, \frac{3}{2})$ reflections in magnetic fields. B.G. represents the background for $(\frac{3}{2}, \frac{3}{2}, \frac{1}{2})$ due to the $\lambda/2$ contamination in the incident beam, which is not detected for $(\frac{1}{2}, \frac{1}{2}, \frac{3}{2})$.

3.2.4 AFQ order in phases II and III

In strong magnetic fields, the AFQ phase is realized, in which an AFM component is expected to be induced with $\boldsymbol{q}_0 = (\frac{1}{2}, \frac{1}{2}, \frac{1}{2})$, as in CeB_6. Figure 6 shows the magnetic Bragg peaks observed in magnetic fields at $(\frac{3}{2}, \frac{3}{2}, \frac{1}{2})$ and $(\frac{1}{2}, \frac{1}{2}, \frac{3}{2})$. These peaks show that the AFM order with $\boldsymbol{q}_0 = (\frac{1}{2}, \frac{1}{2}, \frac{1}{2})$ is induced by the magnetic field, reflecting the underlying AFQ order. Since the intensity of the $(\frac{3}{2}, \frac{3}{2}, \frac{1}{2})$ peak is much higher than that of $(\frac{1}{2}, \frac{1}{2}, \frac{3}{2})$, we can conclude that the field-induced AFM component for $H \parallel [1\bar{1}0]$ is along [001], as in CeB_6.[15] This is consistent with the result of previous studies and the $\langle O_{yz} - O_{zx} \rangle$ order parameter for $H \parallel [1\bar{1}0]$.

In the second scan (labelled "2" in Fig. 5), we measured the $(\frac{3}{2}, \frac{3}{2}, \frac{1}{2})$ peak, corresponding to $\boldsymbol{q}_0$, with decreasing the field. Note that the intensity did not become zero at the II-III boundary at 4 T, and existed even in phase III. Therefore, the magnetic structure of $Ce_{0.5}Pr_{0.1}La_{0.4}B_6$ in phase III for $H \parallel [1\bar{1}0]$ could be such that an AFM modulation with $\boldsymbol{q}_{3,4}$ or $\boldsymbol{q}_{5,6}$ coexists with the AFQ order with $\boldsymbol{q}_0$. Concerning the $\boldsymbol{q}'$ component, although we checked 12 Bragg points equivalent to $(\pm\frac{1}{4}, \pm\frac{1}{4}, 0)$, $(0, \pm\frac{1}{4}, \pm\frac{1}{4})$, and $(\pm\frac{1}{4}, 0, \pm\frac{1}{4})$ in phase III, we could not detect any peak above the background. This result suggests that the Fourier component of the $\boldsymbol{q}'$ vector in phase III is very small. In addition, since the $\boldsymbol{q}_1$ and $\boldsymbol{q}_2$ peaks are decoupled in the first scan in phase III, there is a possibility that the magnetic structure of phase III is described by a single-$\boldsymbol{q}$ ($+\boldsymbol{q}_0$) structure. However, this point is still speculative and requires further study for validity.

3.3 T-x-y phase diagram of $Ce_xR_yLa_{1-x-y}B_6$

The present experimental study clearly shows that the ordered phase of $Ce_{0.5}Pr_{0.1}La_{0.4}B_6$ at zero field is an AFM dipole order with $\boldsymbol{q} = (\frac{1}{4}, \frac{1}{4}, \frac{1}{2})$. If we look back at the specific heat data in Ref. 25, we find that a similar convex $C(T)$ curve in the ordered phase is observed for both Nd doping and Pr doping. Therefore, we conclude that all these phases have the same AFM order param-

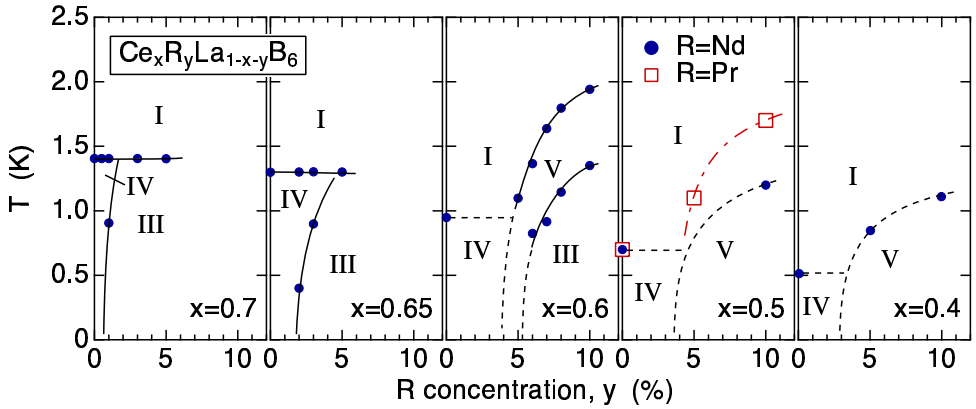

Fig. 7. (Color online) T-x-y phase diagram of $Ce_xR_yLa_{1-x-y}B_6$ for R=Nd and Pr, which we propose from the present study. The dashed lines are speculations.

eter as those in the present case of $Ce_{0.5}Pr_{0.1}La_{0.4}B_6$, where we named it "phase V". We propose in Fig. 7 a modified T-x-y phase diagram of $Ce_xR_yLa_{1-x-y}B_6$ mainly for R=Nd on the basis of the results of several previous studies.[35–38] Specific-heat data not presented in previous reports are shown in Fig. 8. Note that similar a convex $C(T)$ curve is also observed for $x = 0.6$ and $y = 0.05$ for R=Nd.

From the T-y phase diagrams for $x = 0.7$ and 0.65, we see that the transition temperature of phase IV hardly changes with the doping, which could also be the case for $x = 0.6$, 0.5, and 0.4. Then, the increase in the transition temperature in the region $y > 0.05$ is not due to the stabilization of the AFO order of phase IV, as had been anticipated, although it seems continuously connected to $y = 0$ especially for $x = 0.5$ and 0.4. It is more probable that the increase in the transition temperature indicates the appearance of the AFM dipole order, which has been established in the present study of $Ce_{0.5}Pr_{0.1}La_{0.4}B_6$. In addition, since the convex $C(T)$ curve is already observed at a low concentration of $y = 0.05$, it is likely that the AFM order of phase V appears abruptly at a low concentration below $y = 0.05$, which is shown by the dashed curves in Fig. 7.

There is a difference in the T-y phase diagram above and below $x = 0.6$. For $x > 0.6$, phase IV is simply dominated by phase III upon R doping. This is probably because R ion doping favours the incommensurate or commensurate magnetic dipole order with a $\boldsymbol{q}$-vector equal or close to $(\frac{1}{4}, \frac{1}{4}, \frac{1}{2})$,[32,39] which can couple with the AFM order of phase III but not with the AFO order of phase IV.[25] The small energy difference between phases IV and III also favors this coupling, which is supported by the relatively low critical field between phases IV and III for $x > 0.6$ ($H_c^{\text{IV-III}} = 0.6$ T for $x = 0.7$ and 1.5 T for $x = 0.6$).[4] If we proceed with this argument to the region $x < 0.6$, where $H_c^{\text{IV-III}}$ increases ($H_c^{\text{IV-III}} = 1.8$ T for $x = 0.5$ and 2.5 T for $x = 0.4$), we are led to the conclusion that the stabilization of phase III by R doping is suppressed, and another magnetic ordered phase V replaces it. We emphasize that phase III consists of AFM and AFQ components, whereas phase V is purely an AFM phase, as was concluded in Sect. 3.2.2 from the single-$\boldsymbol{q}$ structure and the disappearance of the $\boldsymbol{q}_0$ peak.

With respect to the phase transition in undoped $Ce_xLa_{1-x}B_6$ ($y = 0$) for $x \leq 0.6$, we assigned phase IV (AFO) in Fig. 7. In fact, there are many studies on the compound with $x = 0.5$ where phase IV is interpreted as an ordered phase.[1,2,4,5] On the other hand, some authors do not regard it as an ordered phase.[3,40] To provide more convincing data concerning the existence of the ordered phase, we show in Fig. 9 the specific heat of $Ce_xLa_{1-x}B_6$ for Ce concentrations down to $x = 0.25$; the measurement was performed in zero field using a Quantum Design physical property measurement system. The characteristic of the ordered phase is that $C(T)$ exhibits a power law behavior, approximately $\propto T^2$ for $x \geq 0.6$. With decreasing x, although the peak becomes broader and the exponent slightly decreases, it is clear that some kind of ordering persists even at $x = 0.36$. It has been argued that the critical concentration is $x \sim 0.3$, below which a long-range order cannot develop.[4] We thus consider that some kind of ordering is realized for $x > 0.3$. By contrast, the $C(T)$ curve for $x = 0.25$ below 1 K is far from exhibiting the power law behavior observed for $x > 0.3$, indicating that the long-range order no longer exists.

3.4 Competing nature of the order parameters

Figure 7 shows that a minor perturbation of magnetic ion doping into phase IV induces a sudden transition to an AFM dipole order. At high Ce concentrations of $x > 0.6$, where the AFQ interaction is relatively strong, the AFM order occurs together with the AFQ order (phase III). By contrast, at low Ce concentrations of $x < 0.6$, a different AFM order occurs independently without the AFQ component (phase V), which is described by $\boldsymbol{q} = (\frac{1}{4}, \frac{1}{4}, \frac{1}{2})$. This $\boldsymbol{q}$-vector is widely observed in the antiferromagnetic ordered phases in the RB_6 series, and is considered to result from the Ruderman-Kittel-Kasuya-Yosida (RKKY) interaction, which is associated with the characteristic band structure of the RB_6 system.[41] Thus, we consider that the AFM dipole order of phase V also takes part in the competition be-

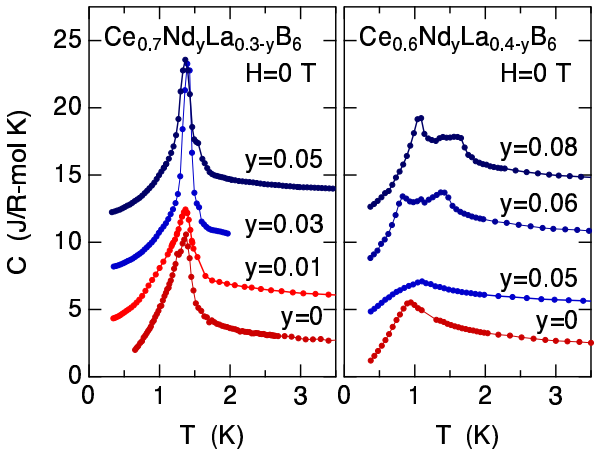

Fig. 8. (Color online) Specific heat of $Ce_xNd_yLa_{1-x-y}B_6$. Data for $y > 0$ are shifted.

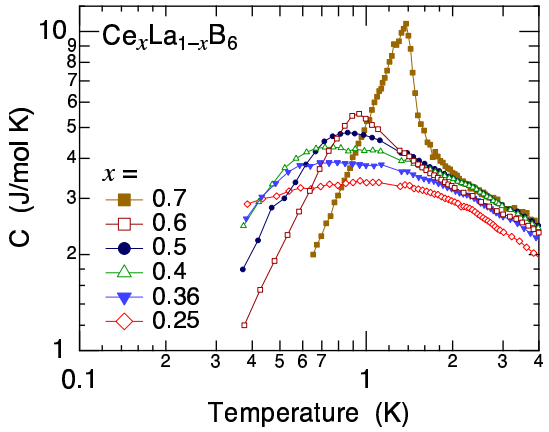

Fig. 9. (Color online) Specific heat of $Ce_xLa_{1-x}B_6$ at zero magnetic field.

tween several order parameters in the $Ce_xLa_{1-x}B_6$ system, in addition to those associated with the AFQ (phase II), AFM+AFQ (phase III), and Γ_{5u}-AFO (phase IV) orders. In magnetic fields, the Γ_{2u}-AFO order, which is associated with the ferromagnetic order and AFQ order, also participates in this competition and further affects the phase diagram. Note that recent inelastic neutron scattering experiments reveal an anomalous spin excitation spectrum, which seems to reflect this strong competition of many types of multipole order parameters.[42,43]

4. Conclusions

A neutron diffraction experiment has been performed on $Ce_{0.5}Pr_{0.1}La_{0.4}B_6$, in which an Γ_{5u}-AFO order with $\boldsymbol{q}_0 = (\frac{1}{2}, \frac{1}{2}, \frac{1}{2})$ has been assumed to occur because of similarities in the macroscopic physical properties to those of $Ce_{0.7}La_{0.3}B_6$. Contrary to this expectation, we observed an unambiguous signal from a magnetic dipole order with $\boldsymbol{q} = (\frac{1}{4}, \frac{1}{4}, \frac{1}{2})$, the same propagation vector frequently realized in rare-earth hexaboride compounds. On the basis of this result, we proposed a T-x-y phase diagram of $Ce_xR_yLa_{1-x-y}B_6$ for R=Nd and Pr, which shows that the order is suddenly switched from AFO to AFM by R ion doping.

Acknowledgements

This work was supported by Grants-in-Aid for Scientific Research (Nos. 21204456, 21102515, and 2430087) from JSPS and MEXT. This work was carried out under the Joint-Use Research Program for Neutron Scattering, Institute for Solid State Physics (ISSP), The University of Tokyo, at the Research Reactor JRR-3, JAEA (proposal no. 10564). The experiment at LLB, France (proposal no. 11742) was carried out with the approval of ISSP (proposal no. 13547).

1) T. Tayama, T. Sakakibara, K. Tenya, H. Amitsuka, and S. Kunii, J. Phys. Soc. Jpn. **66**, 2268 (1997).
2) M. Hiroi, S. Kobayashi, M. Sera, N. Kobayashi, and S. Kunii, J. Phys. Soc. Jpn. **66**, 1762 (1997).
3) O. Suzuki, T. Goto, S. Nakamura, T. Matsumura, and S. Kunii, J. Phys. Soc. Jpn. **67**, 4243 (1998).
4) S. Kobayashi, M. Sera, M. Hiroi, N. Kobayashi, and S. Kunii, J. Phys. Soc. Jpn. **69**, 926 (2000).
5) T. Tayama, S. Honma, K. Tenya, H. Amitsuka, T. Sakakibara, and S. Kunii, Physica B **259-261**, 32 (1999).
6) M. Akatsu, T. Goto, Y. Nemoto, O. Suzuki, S. Nakamura, and S. Kunii, J. Phys. Soc. Jpn. **72**, 205 (2003).
7) R. Shiina, H. Shiba, and P. Thalmeier, J. Phys. Soc. Jpn. **66**, 1741 (1997).
8) H. Kusunose, and Y. Kuramoto, J. Phys. Soc. Jpn. **70**, 1751 (2001).
9) H. Nakao, K. Magishi, Y. Wakabayashi, Y. Murakami, K. Koyama, K. Hirota, Y. Endoh, and S. Kunii, J. Phys. Soc. Jpn. **70**, 1857 (2001).
10) F. Yakhou, V. P. Plakhty, H. Suzuki, S. V. Gavrilov, P. Burlet, L. Paolasini, C. Vettier, and S. Kunii, Phys. Lett. A **285**, 191 (2001).
11) Y. Tanaka, U. Staub, K. Katsumata, S. W. Lovesey, J. E. Lorenzo, Y. Narumi, V. Scagnoli, S. Shimomura, Y. Tabata, Y. Onuki, Y. Kuramoto, A. Kikkawa, T. Ishikawa, and H. Kitamura, Europhys. Lett. **68**, 671 (2004).
12) T. Matsumura, T. Yonemura, K. Kunimori, M. Sera, and F. Iga, Phys. Rev. Lett. **103**, 017203 (2009).
13) T. Matsumura, T. Yonemura, K. Kunimori, M. Sera, F. Iga, T. Nagao, and J. I. Igarashi, Phys. Rev. B **85**, 174417 (2012).
14) J. M. Effantin, J. Rossat-Mignod, P. Burlet, H. Bartholin, S. Kunii, and T. Kasuya, J. Magn. Magn. Mater. **47&48**, 145 (1985).
15) W. A. C. Erkelens, L. P. Regnault, P. Burlet, J. Rossat-Mignod, S. Kunii, and T. Kasuya, J. Magn. Magn. Mater. **63&64**, 61 (1987).
16) K. Iwasa, K. Kuwahara, M. Kohgi, P. Fisher, A. Donni, L. Keller, T. C. Hansen, S. Kunii, N. Metoki, Y. Koike, and K. Ohoyama, Physica B **329-333**, 582 (2003).
17) O. Zaharko, P. Fischer, A. Schenck, S. Kunii, P.-J. Brown, F. Tasset, and T. Hansen, Phys. Rev. B **68**, 214401 (2003).
18) P. Fischer, K. Iwasa, K. Kuwahara, M. Kohgi, T. Hansen, and S. Kunii, Phys. Rev. B **72**, 014414 (2005).
19) K. Kubo and Y. Kuramoto, J. Phys. Soc. Jpn. **73**, 216 (2004).
20) D. Mannix, Y. Tanaka, D. Carbone, N. Bernhoeft, and S. Kunii, Phys. Rev. Lett. **95**, 117206 (2005).
21) H. Kusunose and Y. Kuramoto, J. Phys. Soc. Jpn. **74**, 3139 (2005).
22) K. Kuwahara, K. Iwasa, M. Kohgi, N. Aso, M. Sera, and F. Iga, J. Phys. Soc. Jpn. **76**, 093702 (2007).
23) T. Matsumura, S. Michimura, T. Inami, T. Otsubo, H. Tanida, F. Iga, and M. Sera, Phys. Rev. B **89**, 014422 (2014).
24) A. Kondo, H. Tou, M. Sera, and F. Iga, J. Phys. Soc. Jpn. **76**, 013701 (2007).
25) A. Kondo, T. Taniguchi, H. Tanida, T. Matsumura, M. Sera,

F. Iga, H. Tou, T. Sakakibara, and S. Kunii, J. Phys. Soc. Jpn. **78**, 093708 (2009).
26) F. Iga, N. Shimizu, and T. Takabatake, J. Magn. Magn. Mater. **177-181**, 337 (1998).
27) H. C. Walker, K. A. McEwen, D. F. McMorrow, M. Bleckmann, J.-G. Park, S. Lee, F. Iga, and D. Mannix, Phys. Rev. B **79**, 054402 (2009).
28) C. M. McCarthy and C. W. Thompson, J. Phys. Chem. Solids **41**, 1319 (1980).
29) K. Kuwahara, S. Sugiyama, K. Iwasa, M. Kohgi, M. Nakamura, Y. Inamura, M. Arai, and S. Kunii, Appl. Phys. A **74**, S302 (2002).
30) S. E. Luca, M. Amara, R. M. Galera, F. Givord, S. Granovsky, O. Isnard, and B. Beneu, Physica B **350**, e39 (2004).
31) K. Takahashi, H. Nojiri, K. Ohoyama, M. Ohashi, Y. Yamaguchi, M. Motokawa, and S. Kunii, J. Magn. Magn. Mater. **177-181**, 1097 (1998).
32) J.-M. Mignot, G. André, J. Robert, M. Sera, and F. Iga, Phys. Rev. B **78**, 014415 (2008).
33) A. J. Freeman and J. P. Desclaux, J. Magn. Magn. Mater. **12**, 11 (1979).
34) M. Sera, S. Goto, T. Koshikawa, M.-S. Kim, H. Tou, F. Iga, Y. Mitsukawa, and K. Kojima, J. Phys. Soc. Jpn. **74**, 2691 (2005).
35) A. Kondo, H. Tou, M. Sera, F. Iga, and T. Sakakibara, J. Phys. Soc. Jpn. **76**, 103708 (2007).
36) A. Kondo, H. Tou, M. Sera, F. Iga, T. Morie, and T. Sakakibara, J. Magn. Magn. Mater. **310**, e160 (2007) .
37) A. Kondo, H. Tou, M. Sera, F. Iga, and T. Sakakibara, J. Phys. Soc. Jpn. **77** [suppl. A], 285 (2008).
38) A. Kondo, Dr. Thesis, AdSM, Hiroshima University, Higashi-Hiroshima (2009).
39) J.-M. Mignot, J. Robert, G. André, M. Sera, and F. Iga, Phys. Rev. B **79**, 224426 (2009).
40) S. Nakamura, O. Suzuki, T. Goto, S. Sakatsume, T. Matsumura, and S. Kunii, J. Phys. Soc. Jpn. **66**, 552 (1997).
41) Y. Kuramoto and K. Kubo, J. Phys. Soc. Jpn. **71**, 2633 (2002).
42) G. Friemel, Y. Li, A. V. Dukhnenko, N. Y. Shitsevalova, N. E. Sluchanko, A. Ivanov, V. B. Filipov, B. Keimer, and D. S. Inosov, Nat. Commun. **3**, 830 (2012).
43) H. Jang, G. Friemel, J. Ollivier, A. V. Dukhnenko, N. Y. Shitsevalova, V. B. Filipov, B. Keimer, and D. S. Inosov, Nat. Mater. **13**, 682 (2014).